

Rapid Vapor-Phase Direct Doping for High-Efficiency Solar Cells

Saskia Kühnhold-Pospischil , Bernd Steinhauser, Armin Richter, Elke Gust, and Stefan Janz

Abstract—An alternative boron emitter diffusion process called rapid vapor-phase direct doping (RVD) is studied and applied to n -type silicon solar cells with a tunnel oxide passivated electron contact (TOPCon). The RVD emitter diffusion process occurs under an atmosphere containing only the dopant gas and hydrogen. Thus, compared with standard tribromide diffusion processes, no oxygen is present. Hence, no boron glasses form during the RVD process. Consequently, a faster diffusion process with fewer chemical treatments after the diffusion process compared with standard tribromide processes is possible. In this paper, three different RVD emitter surface dopant concentrations and dopant depths were achieved by process parameter variations. These RVD emitters were applied to TOPCon cells, and their cell characteristics were compared with profiles of TOPCon reference cells with standard boron-diffused emitters. Up to 24.0% cell efficiency, 697.6 mV open-circuit voltage, 41.8 mA/cm² short-circuit current density, and 82.1% fill factor were reached by the best TOPCon cell with an RVD emitter. Nevertheless, compared with the reference, all cells with RVD emitters exhibited efficiency losses. Hence, to further optimize cells with RVD emitters, in-depth characterizations were conducted. The cell efficiency of cells with an RVD emitter is mainly limited by two main reasons: First, effective carrier lifetime degradation was observed, resulting in voltage losses, and second, for RVD diffusion temperatures above 980 °C, a flattening of textured cell surfaces was detected leading to current losses. In order to overcome these issues, an adapted two-step RVD emitter diffusion process is suggested for future experiments.

Index Terms—Boron, diffusion process, photovoltaic cells, p/n -junction.

I. INTRODUCTION

IN THE field of n -type Si photovoltaics, liquid tribromide (BBR₃) as a dopant material is often used to generate boron emitter diffusion in order to form a p/n -junction. During this emitter diffusion process, gases stream along both Si wafer surfaces at temperatures ranging from 800 to 1100 °C within a tube furnace under an ambient atmosphere containing oxygen (O₂) [1]. During the diffusion process, p^+ regions and boron-doped silicate glasses are formed on both wafer surfaces. Thus, after the emitter diffusion process, high-concentrated

hydrofluoric acid is needed to remove boron-doped glasses from both wafer surfaces. In addition, a p/n -junction is usually only needed on one wafer face, and further chemical treatments are required to remove the unwanted p/n -junction from one of the wafer faces. In general, such chemical treatments are cost-intensive and critical in terms of waste treatment.

To form an adequate p/n -junction, the p^+ emitter diffusion process lasts at least 45 min, which is long compared with the duration of other cell-processing steps. A summary of typical durations of boron emitter diffusion steps is given in [2]. Moreover, as an example, multicrystalline materials degrade during high-temperature treatments, and a reduced dwell time at high temperatures might be beneficial.

An alternative to the emitter diffusion process described so far is the so-called rapid vapor-phase direct doping (RVD) emitter [3]. The most significant difference between the standard emitter diffusion and the RVD emitter diffusion is that the process ambient air contains hydrogen (H₂) instead of O₂. For the RVD process, diborane (B₂H₆) is used as the dopant gas, which is diluted in hydrogen. Hence, the formation of a silicate glass layer during the emitter diffusion process is prevented, and the dopant (here boron) is directly transferred from the gas phase into the silicon. Thus, the emitter diffusion time can be reduced, and no chemical treatments to remove unwanted silicate glasses are needed. With that, the RVD emitter profiles can be designed by varying only the B₂H₆ concentrations, diffusion temperatures, and diffusion durations. In addition, the furnace used for the RVD emitter processes presented in this study was arranged such that the emitter formation occurred on one wafer surface only, omitting the need to remove the diffusion layer on the unwanted side. Again, compared with the standard emitter process, a reduction in the amount of chemicals consumed is possible.

Among others, RVD emitters were applied as front junctions in n -type Si solar cells with tunnel oxide passivated contacts (TOPCon) on the rear [4], [5], and they achieved efficiencies as high as 23.3% [6]. Those results indicated that the cells with the RVD emitter suffered from a shallow emitter diffusion profile, which caused higher series resistance losses and additional recombination in the space charge region compared with reference cells with a standard emitter diffusion. Consequently, to avoid the efficiency losses, optimized RVD emitter profiles using longer diffusion times or higher diffusion temperatures than those mentioned above should be employed. These types of RVD diffusion processes have been studied by Kühnhold-Pospischil *et al.* [7]. In that study, emitter surface

Manuscript received April 19, 2018; revised June 8, 2018; accepted July 22, 2018. This work was supported by the European Commission under Grant 609788. (Corresponding author: Saskia Kühnhold-Pospischil.)

The authors are with the Fraunhofer Institute for Solar energy Systems, 79110 Freiburg, Germany (e-mail: saskia.kuehnhold-pospischil@ise.fraunhofer.de; bernd.steinhauser@ise.fraunhofer.de; armin.richter@ise.fraunhofer.de; elke.gust@ise.fraunhofer.de; stefan.janz@ise.fraunhofer.de).

Color versions of one or more of the figures in this paper are available online at <http://ieeexplore.ieee.org>.

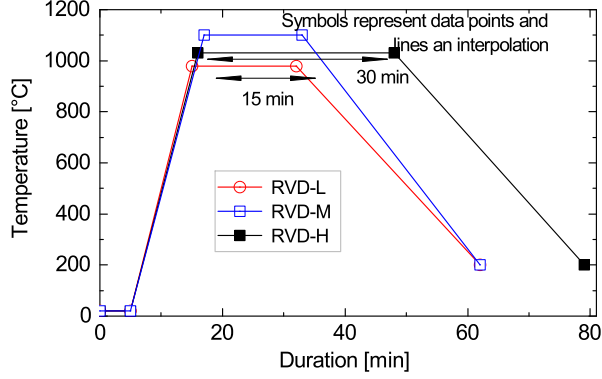


Fig. 1. Temperature profiles of the three RVD diffusion processes [7]. To reach the diffusion temperature, the temperature was ramped from room temperature up to the desired diffusion temperature in approximately 5 min, and after the diffusion process, the sample was cooled from the diffusion temperature to room temperature in approximately 25 min.

concentrations between $5 \times 10^{18} \text{ cm}^{-3}$ and $5 \times 10^{19} \text{ cm}^{-3}$ and a p-n junction depth between $0.18 \mu\text{m}$ and $0.7 \mu\text{m}$ were achieved by varying the diffusion parameters.

In this contribution, each of these RVD emitter profiles was applied as a front-side emitter on high-efficiency *n*-type Si solar cells with TOPCon rear contacts. All cell characteristics are studied and discussed with respect to the RVD emitter profiles.

II. EXPERIMENTAL DETAILS

A. Experimental Design

For the experiments, float-zone, $4''$, *n*-type Si wafers with a base resistivity of $1 \Omega \text{ cm}$ were used. Details about the specific structuring processes, geometries, and metallization of the TOPCon solar cell concept used for the following experiments can be found in [8]. Hereafter, only the emitter variation and process steps relevant for the further discussion are described.

As an emitter reference, standard BBr_3 emitter diffusion was performed within a tube furnace. First, a subgroup of the reference cells received a selective emitter [8]. Prior to the sheet emitter diffusion processes, the wafer surface was textured. For the sheet emitter, a $140 \Omega/\square$ emitter similar to the emitter described by Benick *et al.* was applied [9]. The RVD diffusion process was performed in the *rapid thermal chemical vapor deposition (RTCVD 160)* apparatus [10], [11]. In order to obtain three different surface doping concentrations and doping depths, three different RVD diffusion temperatures (980°C , 1030°C , and 1100°C), two different diffusion temperature durations (15 min and 30 min), and two different process gas fluxes (0.3 slm and 1.5 slm) were applied. All three resulting temperature profiles are shown in Fig. 1. The process gas flux given in slm refers to hydrogen gas mixed with 0.25% B_2H_6 of the dopant gas.

Before the RVD process was conducted, one half of the RVD group with the 980°C diffusion temperature got the same selective emitter as the reference.

A summary of emitter variations is given in Table I. For simplification, a group name was defined for each emitter variation. In the following, *Ref.* refers to reference cells and *RVD* to RVD

TABLE I
RVD DIFFUSION TEMPERATURE, DIFFUSION TEMPERATURE DURATION, AND GAS FLUX OF HYDROGEN MIXED WITH 0.25% B_2H_6 DOPANT GAS

Group name	Sel. emitter	RVD variation			
		RVD emitter	Temp. [$^\circ\text{C}$]	Dur. [min]	H_2 (0.25% B_2H_6) [slm]
<i>Ref.-S</i>	✓	—	—	—	—
<i>Ref.</i>	—	—	—	—	—
<i>RVD-LS</i>	✓	✓	980	15	0.3
<i>RVD-L</i>	—	✓	980	15	0.3
<i>RVD-M</i>	—	✓	1030	30	0.3
<i>RVD-H</i>	—	✓	1100	15	1.5

emitter cells. The additional letter “S” indicates the optional selective emitter. Furthermore, “L” indicates the lowest RVD diffusion temperature (980°C), “M” the medium RVD diffusion temperature (1030°C), and “H” the highest RVD diffusion temperature (1100°C). All resulting group names and additional process parameters are summarized in Table I.

The three different RVD emitter processes were applied to wafers used for the TOPCon cell process and to one additional wafer per RVD emitter variation, which is used to characterize the resulting emitter profile. In total, $18 \times \text{Ref.-S}$ cells, $14 \times \text{Ref.}$ cells, $20 \times \text{RVD-LS}$ cells, $17 \times \text{RVD-L}$ cells, $28 \times \text{RVD-M}$ cells, and $21 \times \text{RVD-H}$ cells were successfully produced.

To measure the resulting emitter profiles, *electrochemical capacitance–voltage profiling* was used [12]. TOPCon cells were characterized using the *transfer length method (TLM)* to determine sheet (R_{sh}) and contact resistances (ρ_c) [13]. Current–voltage (I – V) measurements were used to extract cell efficiencies (η), fill factors (FF), open-circuit voltages (V_{OC}), and short-circuit current densities (J_{SC}). In addition, calibrated *photoluminescence (PL)* measurements to determine τ at 1 sun along all cell structures [14] were taken from the back side of all cells prior to the back-side metallization. Moreover, *reflectance (R)* and absorption measurements were used to determine internal quantum efficiency (IQE) and external *quantum efficiency (EQE)* [15], and the *SunsVoc* [16], [17] method was used to determine the pseudo FF (pFF) and FF_0 as in [18]. Solar cell surfaces were studied using *scanning electron microscopy (SEM)*.

B. Experimental Results

In the following section, the experimental results are presented. The corresponding discussion regarding these results is given in Section III.

All resulting RVD emitter profiles are shown in Fig. 2. As shown from Fig. 2, the lowest surface dopant concentration ($\sim 4.2 \times 10^{18} \text{ cm}^{-3}$) and the lowest dopant depth ($\sim 0.2 \mu\text{m}$) were measured for group *RVD-L*. In contrast, the highest surface doping concentration ($\sim 3 \times 10^{19} \text{ cm}^{-3}$) and highest *p/n*-junction depth ($\sim 0.7 \mu\text{m}$) were measured for group *RVD-H*.

The corresponding R_{sh} values are given in Table II. R_{sh} decreases from approximately $300 \Omega/\square$ to approximately $40 \Omega/\square$ with increasing RVD surface dopant concentration.

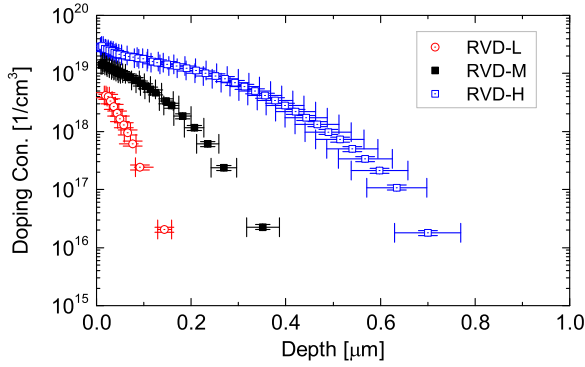


Fig. 2. EVC profiles of RVD emitters produced by varying the diffusion temperature, diffusion temperature duration, and doping gas concentration [7]. The uncertainty of measurement is 10%.

TABLE II
SHEET RESISTANCES (R_{sh}) AND I - V VALUES MEASURED USING
THE BEST SOLAR CELL FOR EACH EMITTER VARIATION

Group name	R_{sh} [Ω/\square]	η [%]	V_{OC} [mV]	J_{SC} [mA/cm ²]	FF [%]
<i>Ref.-S</i>	138.2 ± 0.3	24.6	713.8	41.4	83.2
<i>Ref.</i>	134.1 ± 1.6	24.7*	710.7	42.0	82.9
<i>RVD-LS</i>	316.4 ± 2.4	24.0*	697.6	41.8	82.1
<i>RVD-L</i>	268.4 ± 5.6	23.1	681.4	41.5	81.8
<i>RVD-M</i>	98.9 ± 0.8	23.9*	703.2	41.1	82.8
<i>RVD-H</i>	38.6 ± 1.2	21.3	678.4	38.3	82.0

*independently confirmed by Fraunhofer ISE CalLab.

To analyze the impact of the variation in the RVD emitter on the TOPCon cell characteristics, current–voltage (I - V) measurements were conducted. The best cell efficiencies and corresponding cell parameters measured for both reference groups and all RVD emitter groups are summarized in Table II. The highest η of 24.7% was measured for a reference cell without an additional selective emitter (*Ref.*). For cells with an RVD emitter, the highest η of 24% was observed for a cell with the lowest RVD surface dopant concentration and dopant depth and an additional selective emitter (*RVD-LS*). This cell achieved a V_{OC} of 697.6mV, a J_{SC} of 41.8mA/cm², and an FF of 82.1%. Additionally, a high efficiency of 23.9% was measured for a cell with the medium RVD surface dopant concentration and dopant depth (*RVD-M*). The best cell of the group with the highest RVD surface dopant concentration and dopant depth (*RVD-H*) reached an η of 21.3%.

For a more detailed study of the influence of RVD emitter variations on solar cell parameters, I - V measurements were conducted for all solar cells, and their corresponding cell characteristics are shown as box plots in Fig. 3. As with the cell parameters given in Table II, also the mean values of η , V_{OC} , J_{SC} , and FF were the highest for both reference groups (*Ref.* and *Ref.-S*) compared with those of all RVD emitter cells (see Fig. 3). Both reference groups show nearly identical J_{SC} and FF values. Only V_{OC} is on average ~ 5 mV higher for *Ref.-S* cells. This small V_{OC} gain can be explained by the selective

emitter and is in good agreement with the expected V_{OC} gain of ~ 4 mV estimated based on an area-weighted J_0 calculation.

Moreover, considering the averaged values of the cell parameters for cells with an RVD emitter, the highest η and V_{OC} values were achieved by cells from group *RVD-LS*, the best J_{SC} values by cells from group *RVD-L*, and the highest FF values for group *RVD-H* (see Fig. 3). Considering the averaged cell parameters of all TOPCon cells with an RVD emitter and without the selective emitter (see Fig. 3), η , J_{SC} , and V_{OC} decrease with increasing RVD surface dopant concentration and dopant depth whereas the FF increases.

Since τ can influence cell parameters strongly, calibrated PL measurements were conducted. To limit the influence of optical differences related to the front-side emitter variation, PL measurements were taken from the back side of all TOPCon cells. In Fig. 4, a calibrated PL image of seven reference cells (*Ref.-S*) and a PL image of seven cells with an RVD emitter (*RVD-H*) are shown as examples. As can be seen, the seven solar cells are combined on one single 4" wafer, respectively. In comparison, the cells from group *Ref.-S* show a higher lifetime compared with the cells from group *RVD-H*. Around these solar cells, the wafer surface is not textured and capped during the emitter diffusion process. Hence, no emitter is present. In addition, in the area of the wafer without any RVD emitter, the wafer from group *Ref.-S* shows a higher lifetime compared with the wafer from group *RVD-H*. In addition, in the PL image of the wafer from group *RVD-H* [see Fig. 4(b)], an area of bad τ values with a triangular shape can be seen. Similar observations were shown by Kühnhold-Pospischil *et al.* [7]. In that study, it is shown that these structures appear after high-temperature treatments in the *RTCVD 160* even without any additional dopant gases.

A summary of the averaged τ values for all cells is given in Fig. 5 on a logarithmic scale. Again, the highest τ values are reached by both reference groups (*Ref.-S* and *Ref.*), and the highest τ values for cells with an RVD emitter are reached by *RVD-LS*. For all other RVD cells, τ seems to decrease with increasing RVD surface dopant concentration and dopant depth.

To further investigate the decrease in J_{SC} values with increasing RVD surface dopant concentration and dopant depth, R and QE values were measured for all solar cells [15]. Representative examples of the corresponding results can be seen in Fig. 6. A comparison between the reference cells [see Fig. 6(a)] and the RVD emitter cell *RVD-LS* [see Fig. 6(a) and (b)] shows that each of the R , IQE , and EQE curves are nearly identical. A comparison of R between all RVD emitter cells shows that R increases with increasing RVD surface dopant concentration and dopant depth for each wavelength between 200 nm and 400 nm and 600 nm and 1100nm. Between 1100 nm and 1200 nm, R decreases slightly with increasing RVD surface dopant concentrations and dopant depth. Also, the IQE for each wavelength between 200 nm and 500 nm decreases with increasing RVD surface dopant concentrations and dopant depth.

To further analyze the changes in J_{SC} , R , and QE , the surfaces of the reference cells and all RVD emitter cells were studied using SEM. In Fig. 7, the SEM micrographs of a reference cell (*Ref.-S*) surface and the SEM micrographs of a cell surface from group *RVD-H* are given as examples. A compar-

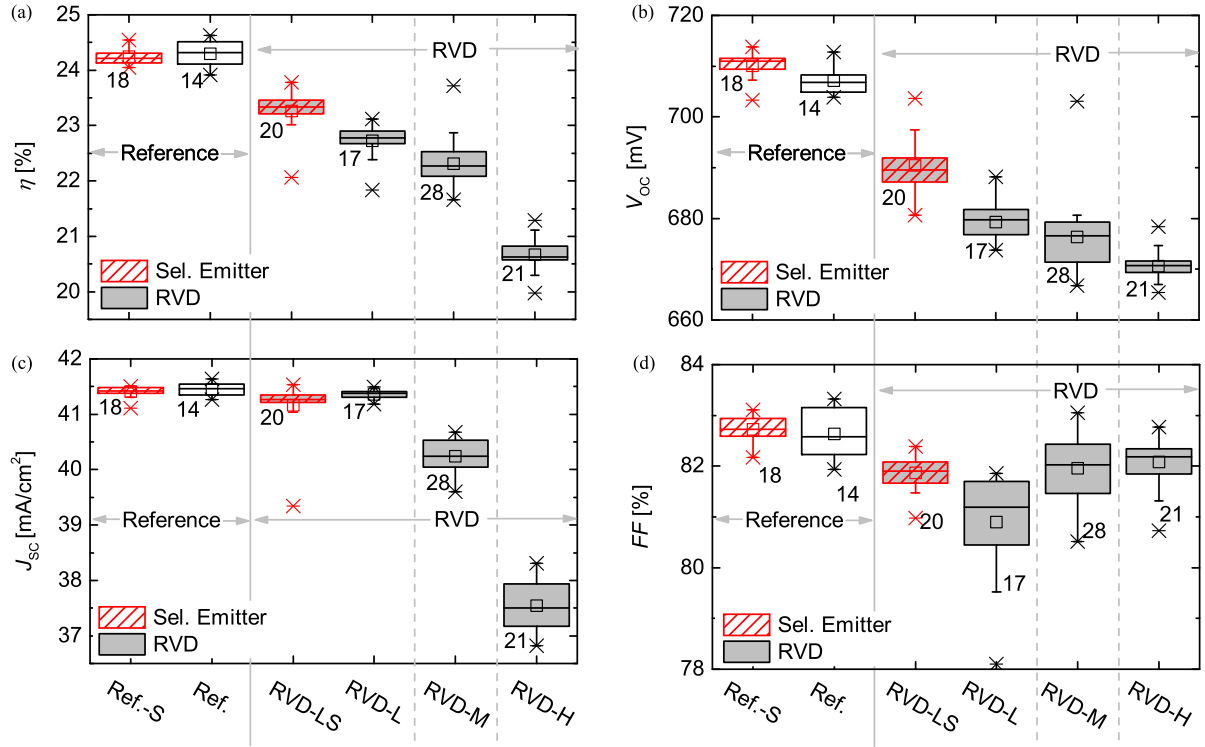


Fig. 3. Box plot of efficiencies (η) in (a), open-circuit voltages (V_{OC}) in (b), short-circuit current densities (J_{SC}) in (c), and fill factors (FF) in (d) for TOPCon cells with a standard BBr_3 -diffused emitter with and without a selective emitter (*Ref.-S* and *Ref.*), and TOPCon cells with three different RVD emitter profiles again with and without an additional selective emitter (*RVD-LS*, *RVD-L*, *RVD-M*, and *RVD-H*). The results were obtained by using the I - V measurement method. The number next to each data point is the number of cells used for the statistical analysis. The lower and upper limits of each box represent the 25% and 75% percentile, respectively. Whiskers are limited by the corresponding interquartile distance times the factor 1.5. Data points outside the whiskers are defined as spikes (represented as crosses). Inside quartiles, the median (horizontal bar) and average (square) are given.

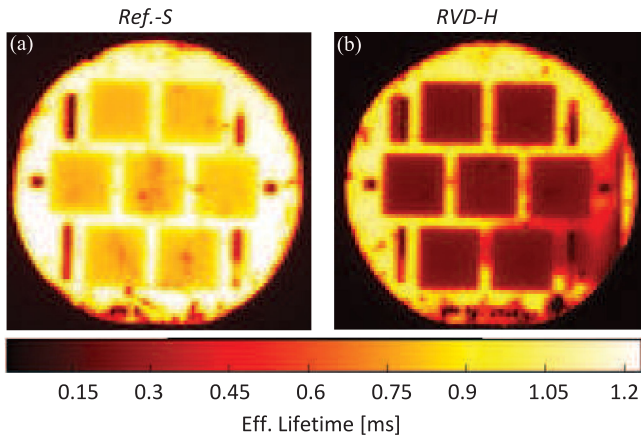


Fig. 4. PL images taken at 1 sun of a reference wafer with a selective emitter (*Ref.-S*) in (a) and a wafer with an RVD emitter (*RVD-H*) in (b). Each wafer has seven TOPCon cells. Next to the cells, TLM structures are visible as four vertical black stripes and two small rectangles on each wafer.

ison among the micrographs of all emitter groups produced reveals that the surface texture flattened with increasing RVD surface dopant concentrations and dopant depth. No difference was visible between the reference (*Ref.-S* and *Ref.*) and the RVD emitter cells from group *RVD-LS* and group *RVD-L* (results are not shown here).

To further understand the FF losses, which are mainly visible for solar cells from group *RVD-L*, the pFF and FF_0 were

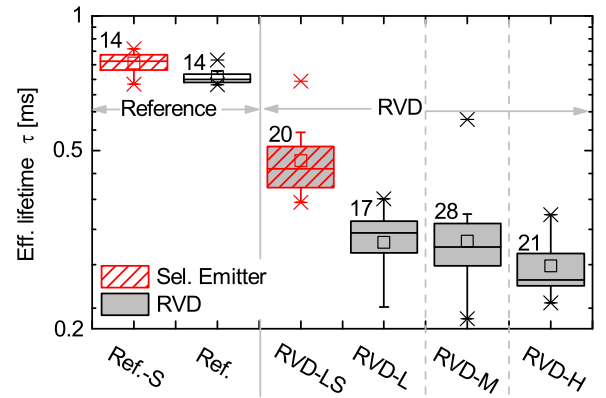


Fig. 5. Effective carrier lifetimes (τ) obtained using the PL method (at 1 sun) for TOPCon cells with a standard BBr_3 -diffused emitter with and without a selective emitter (*Ref.-S* and *Ref.*) and TOPCon cells with three different RVD emitter profiles again with and without an additional selective emitter (*RVD-LS*, *RVD-L*, *RVD-M*, and *RVD-H*). The number next to each data point is the number of cells used for the statistical analysis. The lower and upper limits of each box represent the 25% and 75% percentile. Whiskers are limited by the corresponding interquartile distance times the factor 1.5. Data points outside the whiskers are defined as spikes (represented as crosses). Inside quartiles, the median (horizontal bar) and average (square) are given.

determined for all cells. As discussed by Greulich *et al.* [19], the difference between pFF and FF is related to series resistance (R_S) losses. This difference is shown in Fig. 8 (a) for all cells. $pFF - FF$ values for cells from group *RVD-L*, group *RVD-M*,

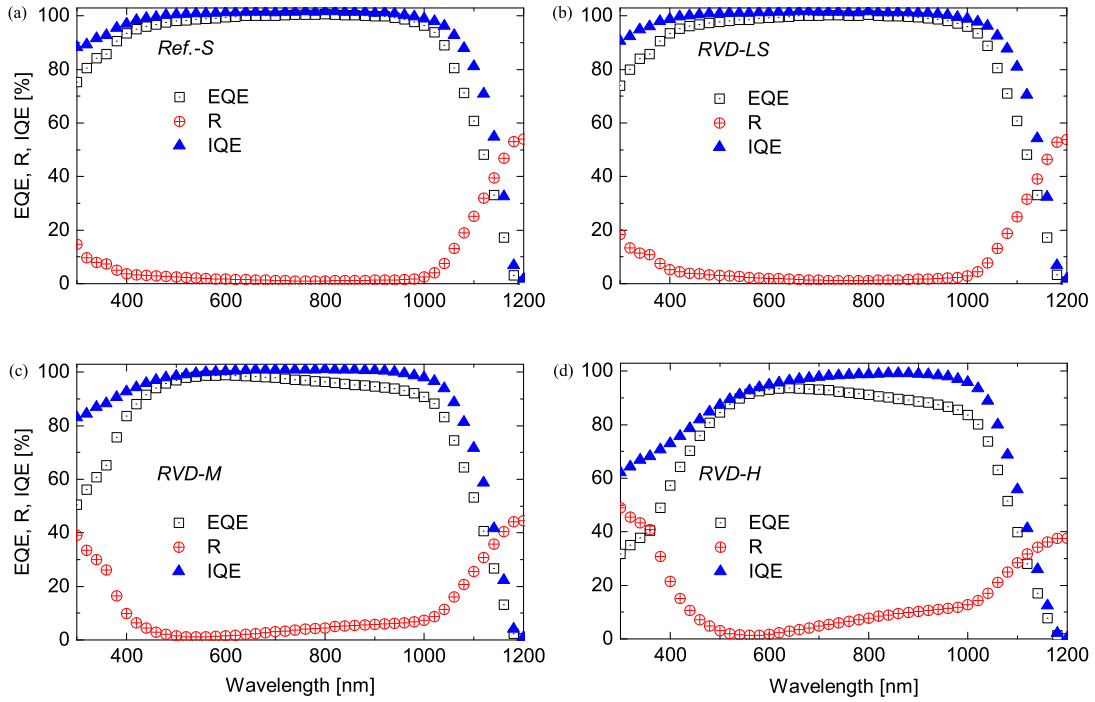


Fig. 6. Representative reflectivity (R), IQE , and EQE values as a function of wavelength for a cell from group $Ref.-S$ (a), a cell from group $RVD-LS$ in (b), a cell from group $RVD-M$ in (c), and a cell from group $RVD-H$ in (d).

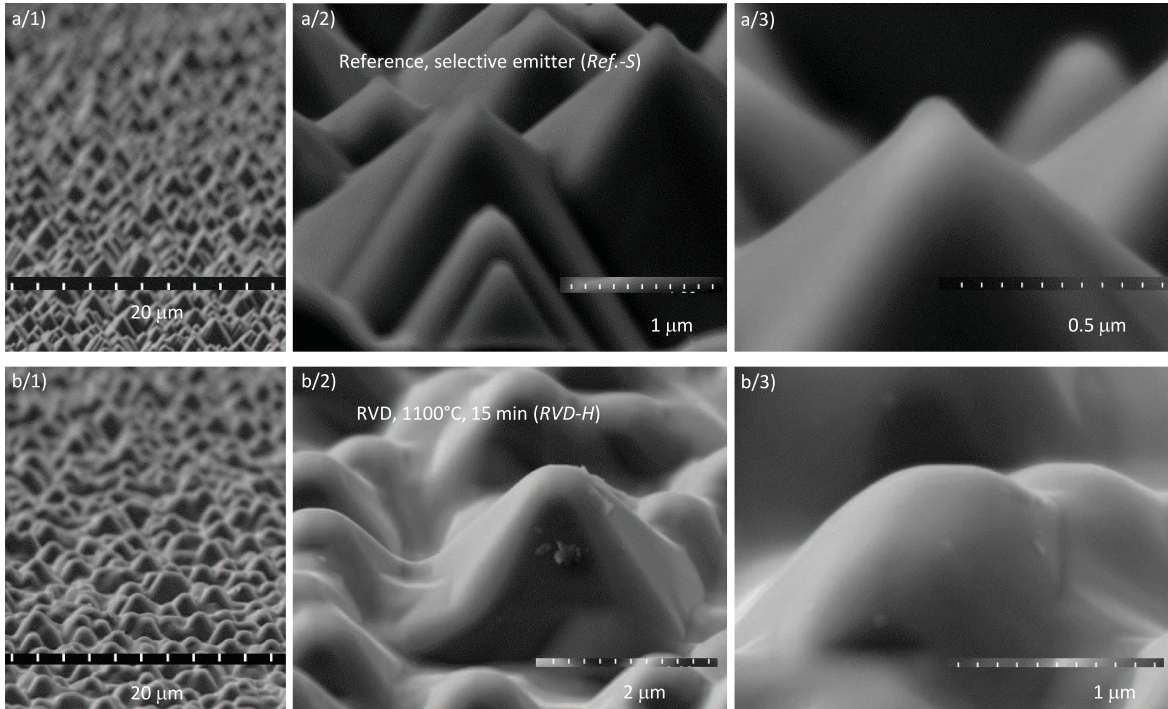


Fig. 7. SEM micrographs of TOPCon cell surfaces in (a/1) to (a/3) of a cell from group $Ref.-S$ and in (b/1) to (b/3) of a cell from group $RVD-H$.

and group $RVD-H$ decrease with increasing RVD surface dopant concentrations and dopant depth. The $pFF - FF$ values from $RVD-LS$ lie between the $pFF - FF$ values for cells from group $RVD-L$ and group $RVD-M$. Because the base resistivity and the metallization are identical for all solar cells, differences in R_S

can be attributed to differences in R_{sh} and ρ_c on the front side of the solar cells. Therefore, the R_{sh} (given in Table II) and ρ_c values are important to further understand the origin of R_S losses. The ρ_c values for all cells are given in Fig. 9. The ρ_c values measured for group $Ref.-S$ and group $RVD-LS$ are on a

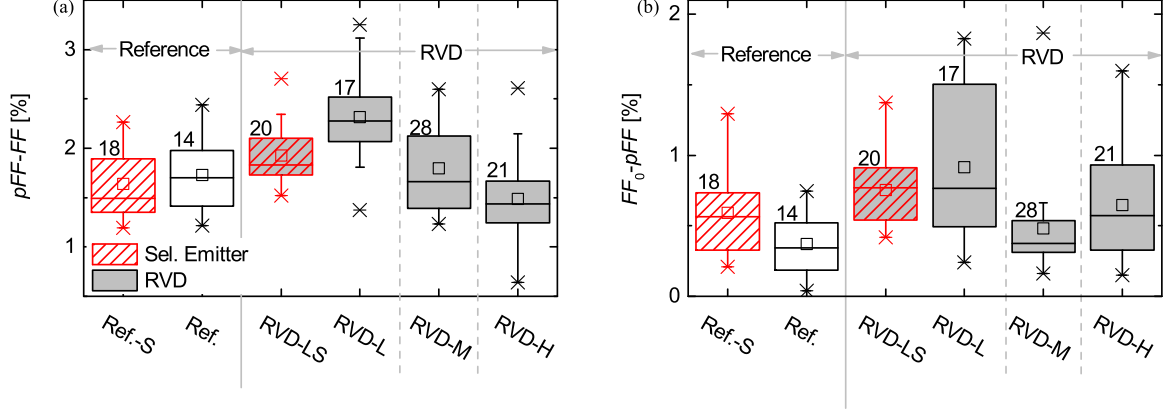


Fig. 8. Difference between pFF and FF in (a) and the difference between FF_0 and pFF in (b) are shown for all emitter variations. pFF and FF_0 were estimated using the *SunsVoc* method. Numbers given next to the data points show the number of cells used for the statistical analysis. The lower and upper limits of each box represents the 25% and 75% percentile, respectively. Whiskers are limited by the corresponding interquartile distance times the factor 1.5. Data points outside the whiskers are defined as spikes (represented as crosses). Inside quartiles, the median (horizontal bar) and average (square) are given.

similar low level. *Ref.* and all other RVD cells reveal higher ρ_c values. Furthermore, ρ_c decreases with increasing RVD surface dopant concentrations and dopant depth. The ρ_c for group *Ref.* is similar to that of *RVD-M*.

The difference between FF_0 and pFF is related to carrier recombination in the space charge region (j_{02}), ohmic shunts (R_p), or other injection-dependent losses [19]. The difference between FF_0 and pFF is shown in Fig. 8 (b). The $FF_0 - pFF$ values from group *RVD-M* and group *RVD-H* are similar to those of both reference groups. Cells from group *RVD-LS* and group *Ref.-L* reveal higher $FF_0 - pFF$ values than those of all other cells.

In the following section, the experimental results are discussed.

III. DISCUSSION

Efficiency losses observed for all RVD emitter TOPCon cells can mainly be attributed to losses in V_{OC} observed for all RVD groups, J_{SC} losses for the RVD groups *RVD-M* and *RVD-H*, and minor influence is attributed to FF losses. V_{OC} and J_{SC} values decreased with increasing RVD surface dopant concentrations and dopant depth, while the FF increased with increasing RVD surface dopant concentrations and dopant depth.

Additionally, τ values of all solar cells decreased with increasing RVD surface dopant concentrations and dopant depth. The trend of τ is similar to the trend observed for V_{OC} when representing all τ values in a logarithmic scale. A connection between V_{OC} and Δn is given as

$$V_{OC} = V_T \ln \left(\frac{\Delta n (N_A + \Delta n)}{n_i^2} \right) \quad (1)$$

whereat V_T is the thermal voltage, N_A is the doping concentration of the base, n_i is the intrinsic carrier concentration, and Δn is the excess carrier density. At 1-sun illumination, a relation between V_{OC} and τ is derived from (1) and is given as

$$V_{OC} \propto \ln(\Delta n) \propto \ln(\tau). \quad (2)$$

Thus, Equation (2) describes the observed correlation between V_{OC} and τ measured at 1 sun. To further verify the correlation between τ and V_{OC} , the *implied* V_{OC} was calculated using Equation (1). To this end, the excess carrier density (Δn) was extracted from the calibrated PL measurements. The calculated *implied* V_{OC} values and the measured V_{OC} values are nearly identical (not shown here). Hence, the decrease in V_{OC} with increasing RVD surface dopant concentrations and dopant depth is connected to the degradation observed for τ . Furthermore, the variance in V_{OC} observed for all RVD groups is high compared with the variance of V_{OC} measured at cells from groups *Ref.-S* and *Ref.* Due to the connection between V_{OC} and τ , this variance can be explained with the inhomogeneously distributed τ values along all wafers after the RVD process (see Fig. 4). The origin of the V_{OC} or τ degradation is not yet fully understood. Likely, the cleanliness and handling technique of the Si wafer material prior to the RVD process and the cleanliness of the *RT-CVD 160* tool play a major role in the degradation outcome. Nevertheless, to better understand degradation processes during RVD emitter diffusion, a separation between carrier recombination losses related to the bulk or induced by the RVD emitter itself is needed.

The higher averaged V_{OC} measured for *RVD-LS* compared with the averaged V_{OC} values of all other RVD cells can be explained by higher shielding of minority carriers under the contact fingers due to the selective emitter, resulting in better τ values.

A decrease in the J_{SC} values with increasing RVD surface dopant concentrations and dopant depth is related to the flattening of the textured front surface during the RVD emitter diffusion process, leading to a reduction in EQE (see Figs. 6 and 7). Such flattening of pyramids in a H_2 -containing atmosphere can be explained in analogy to [20]. In that study, Si surface transformations were observed when exposing Si surfaces to H_2 atmospheres at temperatures between 1000 and 1100 °C and were explained by Si atomic surface diffusion processes [20]. Since the diffusion coefficient is higher for convex structures than for concave structures, the edges are rounded [20].

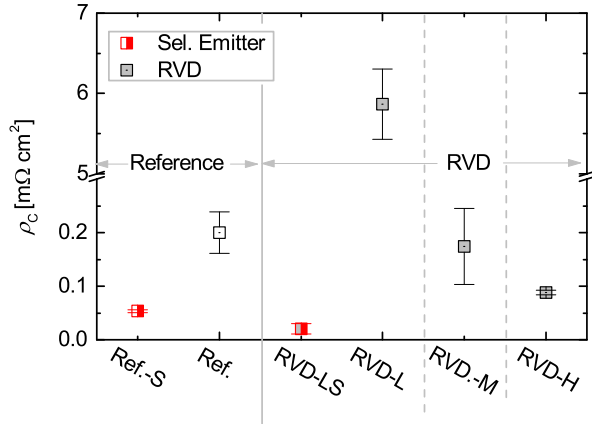


Fig. 9. Contact resistances ρ_c for both reference groups and all RVD emitter cells obtained using the TLM method.

Additional J_{SC} losses are connected to IQE losses in the short-wavelength range as the RVD surface dopant concentrations and dopant depth increases. These losses are most probably connected to an enhancement of carrier recombination in the emitter itself.

Another reason for η losses observed for RVD emitter cells is related to FF losses. With increasing RVD surface dopant concentration and dopant depth for all RVD cells without a selective emitter, FF values increase, while R_{sh} and ρ_c decrease (see Table II and Figs. 3 and 9). The lowest ρ_c values were measured for cells with an additional selective emitter (groups *RVD-LS* and *Ref.-S*). Thus, the FF losses observed are connected to R_S and ρ_c losses, which also fit to the behavior of the $pFF - FF$ values [see Fig. 8(a)]. The relatively high R_{sh} values observed for groups *RVD-LS* and *RVD-L* compared with those of all other groups are related to a relatively low surface concentration of charge carriers. Additional FF losses for these groups can be explained by an increased recombination in the space charge region due to the shallow lowly doped emitter. This is supported by the increase in $FF_0 - pFF$ corresponding to an increase in J_{02} .

The main intention of the present work was to obtain three characteristic emitter profiles and their application in TOPCon cells. For this purpose, three RVD process parameters in three experiments (*RVD-L*, *RVD-M*, and *RVD-H*) were varied (see Section II-A), which, however, implies that a well-defined correlation between process parameter changes with changes in the characteristics studied in this contribution is not possible. Nevertheless, only the diffusion temperature is varied for all three experiments whereat the diffusion temperature duration and the process gas flux are hold constant for two experiments, respectively. Thus, considering the observed changes in the sample characteristics in dependence with each experimental parameter (diffusion temperature, diffusion temperature duration, and process gas flux), the process parameter with the main impact can be assumed. As discussed so far, η , V_{OC} , J_{SC} , τ , and ρ_c are the highest for group *RVD-L*, lower for group *RVD-M*, and lowest for group *RVD-H*. For the FF , the behavior is vice versa. This “three-step behavior” correlates only with the three different diffusion temperatures applied. These considerations

fit, e.g., to the observed temperature-induced τ degradation described by Kühnhold-Pospischil *et al.* [7]. Nevertheless, to study the influence of diffusion temperature, diffusion temperature duration, and process gas fluxes on the characteristics shown in this contribution, further studies are needed.

In conclusion, lowest V_{OC} and J_{SC} losses were observed for the lowest RVD surface dopant concentration and dopant depth applied. Nevertheless, higher FF s can be achieved with the highest RVD dopant surface concentration and dopant depth studied in this contribution. Interestingly, as shown by Lee and Wu, the flattening of Si surface structures in hydrogen containing atmospheres increases with increasing diffusion temperature, increasing temperature treatment duration, and process pressure [20]. In that study, it is shown that the flattening process occurs with the fourth root of time. Thus, to reduce J_{SC} losses for RVD emitter cells, the diffusion temperature should be as low and short as possible. Hence, a two-step diffusion process might be a solution to achieve high FF and J_{SC} values. As a first step, a highly doped surface should be produced using high temperatures under highly doped H_2 -containing atmospheres for a short time. As a next step, a longer diffusion step under a nitrogen atmosphere without dopants, for example, could follow for a longer time to achieve a certain emitter profile.

IV. SUMMARY

In this paper, solar cells with an RVD boron emitter reaching cell parameters as high as $\eta = 24.0\%$, $V_{OC} = 697.6$ mV, $J_{SC} = 41.8$ mA/cm², and $FF = 82.1\%$ have been presented. Compared with BBr_3 standard emitter diffusion processes, the RVD emitter formation requires less time, and fewer chemical posttreatments after diffusion are needed. Three different emitter profiles have been processed, and their corresponding influence on the solar cell characteristics has been analyzed. Solar cells with RVD emitters studied in this publication were mainly limited by J_{SC} and V_{OC} losses. Both J_{SC} and V_{OC} values decreased with increasing RVD surface dopant concentration and dopant depth. J_{SC} losses can be explained by the flattening of pyramids during the diffusion process in a H_2 -containing atmosphere and by enhanced recombination of charge carriers within the emitter. The losses in V_{OC} are related to τ degradation. To avoid these J_{SC} and V_{OC} losses, lower diffusion temperatures and diffusion times might be preferable. Nevertheless, the FF increased with increasing surface dopant concentration and dopant depth, which is related to lower R_{sh} and ρ_c values. Thus, to further optimize cell parameters with RVD emitters, a two-step diffusion process is proposed.

ACKNOWLEDGMENT

The authors thank A. Leimenstoll, F. Schätzle, S. Seitz, A. Seiler, H. Steidl, D. Amiri, E. Schäffer, K. Zimmermann, L. Kraus, A. Ivanov, and U. Heitmann for their contributions during solar cell processing and solar cell characterizations.

REFERENCES

- [1] J. Benick, *High-Efficiency N-Type Solar Cells with a Front Side Boron Emitter*. München, Germany: Verlag Dr. Hut, 2011.
- [2] M. Li *et al.*, “Numerical simulation of doping process by BBr₃ tube diffusion for industrial *n*-type silicon wafer solar cells,” *IEEE J. Photovolt.*, vol. 7, no. 3, pp. 755–762, May 2017.
- [3] Y. Kiyota *et al.*, “Ultra-thin-base Si bipolar transistor using rapid vapor-phase direct doping (RVD),” *IEEE Trans. Electron Devices*, vol. 39, no. 9, pp. 2077–2081, Sep. 1992.
- [4] F. Feldmann, M. Bivour, C. Reichel, M. Hermle, and S. W. Glunz, “Passivated rear contacts for high-efficiency *n*-type Si solar cells providing high interface passivation quality and excellent transport characteristics,” *Sol. Energy Mater. Sol. Cells*, vol. 120, pp. 270–274, 2014.
- [5] S. Glunz *et al.*, “The irresistible charm of a simple current flow pattern 25% with a solar cell featuring a full-area back contact,” in *Proc. 31st Eur. Photovolt. Sol. Energy Conf. Exhib.*, 2015, pp. 259–263.
- [6] S. Lindekugel *et al.*, “Emitters grown by rapid vapour-phase direct doping for high efficiency solar cells,” in *Proc. 31st Eur. Photovolt. Sol. Energy Conf. Exhib.*, 2015, pp. 429–432.
- [7] S. Kühnhold-Pospischil *et al.*, “Rapid vapor-phase direct diffused emitter for solar cell applications,” in *Proc. 33th Eur. Photovolt. Sol. Energy Conf. Exhib.*, 2017.
- [8] A. Richter *et al.*, “*n*-type Si solar cells with passivating electron contact: Identifying sources for efficiency limitations by wafer thickness and resistivity variation,” *Sol. Energy Mater. Sol. Cells*, vol. 173, pp. 96–105, 2017.
- [9] J. Benick *et al.*, “High-efficiency *n*-type silicon solar cells with front side boron emitter,” in *Proc. 24th Eur. Photovolt. Sol. Energy Conf. Exhib.*, 2009, pp. 863–870.
- [10] F. R. Fallor and A. Hurrle, “High-temperature CVD for crystalline-silicon thin-film solar cells,” *IEEE Trans. Electron Devices*, vol. 46, no. 10, pp. 2048–2054, Oct. 1999.
- [11] S. Reber, C. Haase, N. Schillinger, S. Bau, and A. Hurrle, “The RTCVD160—A new lab-type silicon CVD processor for silicon deposition on large area substrates,” in *Proc. 3rd IEEE World Conf. Photovolt. Energy Convers.*, 2003, vol. 2, pp. 1368–1371.
- [12] E. Peiner, A. Schlachetzki, and D. Krüger, “Doping profile analysis in Si by electrochemical capacitance-voltage measurements,” *J. Electrochem. Soc.*, vol. 142, no. 2, pp. 576–580, 1995.
- [13] G. Reeves and H. Harrison, “Obtaining the specific contact resistance from transmission line model measurements,” *IEEE Electron Device Lett.*, vol. EDL-3, no. 5, pp. 111–113, May 1982.
- [14] J. Giesecke, M. Schubert, B. Michl, F. Schindler, and W. Warta, “Minority carrier lifetime imaging of silicon wafers calibrated by quasi-steady-state photoluminescence,” *Sol. Energy Mater. Sol. Cells*, vol. 95, no. 3, pp. 1011–1018, 2011.
- [15] B. Fischer, *Loss Analysis of Crystalline Silicon Solar Cells Using Photoconductance and Quantum Efficiency Measurements*. Göttingen, Germany: Cuvillier, 2003.
- [16] R. Sinton and A. Cuevas, “A quasi-steady-state open-circuit voltage method for solar cell characterization,” in *Proc. 16th Eur. Photovolt. Sol. Energy Conf.*, 2000, pp. 1152–1155.
- [17] A. McEvoy, T. Markvart, L. Castañer, T. Markvart, and L. Castaner, *Practical Handbook of Photovoltaics: Fundamentals and Applications*. Amsterdam, The Netherlands: Elsevier, 2003.
- [18] M. A. Green, *Solar Cells: Operating Principles, Technology, and System Applications*. Englewood Cliffs, NJ, USA: Prentice-Hall, 1982.
- [19] J. Greulich, M. Glatthaar, and S. Rein, “Fill factor analysis of solar cells’ current–voltage curves,” *Prog. Photovolt.: Res. Appl.*, vol. 18, no. 7, pp. 511–515, 2010.
- [20] M.-C. Lee and M. C. Wu, “Thermal annealing in hydrogen for 3-D profile transformation on silicon-on-insulator and sidewall roughness reduction,” *J. Microelectromech. Syst.*, vol. 15, no. 2, pp. 338–343, 2006.